Draft version July 12, 2017
Preprint typeset using LaTeX style emulateapj v. 12/16/11

MID-INFRARED VARIABILITY OF CHANGING-LOOK AGN

Zhenfeng Sheng[1†], Tinggui Wang[1‡], Ning Jiang[1], Chenwei Yang[1], Lin Yan[2], Liming Dou[3], Bo Peng[1]

Draft version July 12, 2017

ABSTRACT

It is known that some active galactic nuclei (AGNs) transited from type 1 to type 2 or vice versa. There are two explanations for the so-called changing look AGNs: one is the dramatic change of the obscuration along the line-of-sight, the other is the variation of accretion rate. In this paper, we report the detection of large amplitude variations in the mid-infrared luminosity during the transitions in 10 changing look AGNs using WISE and newly released NEOWISE-R data. The mid-infrared light curves of 10 objects echoes the variability in the optical band with a time lag expected for dust reprocessing. The large variability amplitude is inconsistent with the scenario of varying obscuration, rather supports the scheme of dramatic change in the accretion rate.

1. INTRODUCTION

Active galactic nuclei (AGNs) are empirically classified into Type 1 and Type 2 according to the emission lines width. Type 1 AGNs show both broad and narrow emission lines in spectra while Type 2 display only narrow lines. Intermediate types, 1.5 and 1.8/1.9, were further introduced depending on the relative strength of broad and narrow lines (Osterbrock et al. 1977, 1981). Whereas the early discovery of broad lines in the polarized spectra of type 2 AGNs (Antonucci & Miller, 1985), together with other evidence, led to a unification scheme (Antonucci et al. 1993): two types of AGNs are intrinsically the same but differ only in the orientation of the torus-like obscurer. In this scheme, Type 1 AGNs are viewed face-on so that we look directly into the central accretion disk and the broad emission line region (BLR), while Type 2 are viewed edge-on and our line of sight to the central engine is blocked by a putative dusty torus. Despite the success of unification model, there are arguments that at least some type-2 AGNs are intrinsic, lacking of broad lines because of inadequate accretion rate (Shi et al. 2010; Bianchi et al. 2012; Pons et al. 2014).

Some AGNs are known to transit between Type 1 and Type 2 (e.g. from Type 2 to Type 1, Khachikian & Weedman 1971; from Type 1 to Type 2, Peterson & Perez 1984). These objects are called changing-look (CL) AGNs, featuring emerging or disappearing broad emission lines (BELs). There are some notable CL AGNs reported so far. Mrk 590 changed from Seyfert 1.5 to 1.0 and back to 2 over several decades (Denney et al. 2014). NGC 2617 was reported to have changed from Type 1.8 to Type 1 (Shappee et al. 2014), but recently it likely has a new outburst and continues brightening (Oknyansky et al. 2017). More recently, it is reported that Mrk 1018 changed back to Type 1.9 after 30 years being a as Type 1 (McElroy et al. 2016).

Although the origin of the CL behavior is unwell understood, various scenarios have been proposed. In one scenario, CL is interpreted in the context of unification scheme, and disappearing or emerging of BELs are ascribed to variable obscurer moving in and out of the line of sight (Goodrich 1989). In the other scenario, CL is attributed to the dramatic changes in accretion rate, arising from disk instability or even the tidal disruption, in which the continuum and broad lines should respond immediately while narrow lines remain nearly unchanged. LaMassa et al. (2015) demonstrated that both the photometric and spectral properties of CL AGN J0159+0033 cannot be explained by the unification paradigm, but suggested that accretion power decreases. Macleod et al. (2016) undertook a systematic search for CL AGNs using SDSS and Pan-STARRS1 and found 10 CL AGNs. Runnoe et al. (2016) recently reported a new CL AGN J1011+5442 through Time Domain Spectroscopic Survey (TDSS). Both Macleod et al. (2016) and Runnoe et al. (2016) favor accretion rate change interpretation.

In this work, we focus on the mid-infrared variability (MIR) of CL AGNs and its application in testing CL scenarios. Since infrared emission is produced by dust heated by the UV radiation of accretion disk, it would respond to the variation of the latter with a time lag of order of years. Jun et al. (2015) used the mid-infrared echo to confirm that PG 1302-102's optical periodic variability is accretion disk driven. Besides, infrared emission is much less affected by dust extinction than optical radiation as the opacity decreases steeply towards long wavelength. Moreover, the size of torus is much larger than those of BLR and accretion disk. Therefore, the effect of obscuration by a dusty cloud in optical and infrared would be very different. This would allow us to test the two different scenarios.

We report a discovery of a significant infrared variation of 8 CL AGNs. The outline of the paper is as follows. In §2, we describe the CRTS data, WISE/NEOWISE data and SDSS data used in this study, along with initial data processing. In §3, we present some details of each source and shortly review their properties. In §4, we simply

[1] CAS Key Laboratory for Researches in Galaxies and Cosmology, University of Sciences and Technology of China, Hefei, Anhui 230026, China; †shengzf@mail.ustc.edu.cn; ‡twang@ustc.edu.cn
[2] Caltech Optical Observatories, Cahill Center for Astronomy and Astrophysics, California Institute of Technology, Pasadena, CA 91125, USA; Infrared Processing and Analysis Center, California Institute of Technology, Pasadena, CA 91125, USA
[3] Center for Astrophysics, Guangzhou University, Guangzhou 510006, China; Astronomy Science and Technology Research Laboratory of Department of Education of Guangdong Province, Guangzhou 510006, China

discuss the possible scenarios, and then we come to a conclusion in §5. We adopt a flat ΛCDM cosmology with $H_0 = 70kms^{-1}Mpc^{-1}$ and $\Omega_m = 0.27$.

2. DATA

In this section, we will introduce the datasets used to construct the optical/MIR light curves and the sample selection. Our investigation is mainly based on V-band data from Catalina Real-Time Transient Survey (CRTS, Drake et al. 2009), and MIR data from Wide-field Infrared Survey Explorer (WISE; Wright et al. 2010) and newly released Near-Earth Object WISE Reactivation mission (NEOWISE-R; Mainzer et al. 2014). CRTS is one of the largest time domain optical survey currently operating, covering ∼33000 deg^2 with a baseline of 8 years and ∼250 exposures per year for each target. The survey is performed using unfiltered light but calibrated to a V-band zero-point. We have rejected the data points with large uncertainties (>0.2mag) and spurious points (usual outliers). Then we have binned these data using the median value. The WISE has surveyed the full-sky 1.2 times in four infrared bands W1, W2, W3, W4 centered at 3.4, 4.6, 12, and 22 μm from January to September 2010, on which its cryogen used to cool the W3 and W4 instruments was exhausted. Afterwards it was extended an additional 4 months using W1 and W2, and then placed in hibernation on 2011 February 1. On 2013 October 3 it is reactivated and named NEOWISE-R, using only W1 and W2 (Mainzer et al. 2014). So there is a ∼3.5 years gap in both W1 and W2 band light curves. WISE scans a full sky area every half year and thus yielded 6-7 times of observations for each object up to the most recent public catalog. Firstly, we have removed bad data points of low image quality ('qi_fact'<1), small separation to South Atlantic Anomaly ('SAA'<5) and flagged moon masking ('moon_mask'=1). Then we group the data every half year as in our previous work (Jiang et al. 2012, 2016) and bin the data using median value. Besides we also collect the Stripe 82 multi-epoch data (Abazajian et al. 2009) to visually compare to CRTS V-band data.

We collect the CL AGNs reported in literature as much as possible to investigate their MIR behavior. These sources are then screened according to following criteria:

(1) Seyfert galaxies or quasars which changed from Type 1 to Type ≥1.8 or from Type≥1.8 to Type 1. Immediate types, 1.2 or 1.5 are abandoned because they may be partially obscured, complicating the interpretation.

(2) Variability amplitude is larger than 0.4 mag at 10σ significance in either W1 or/and W2 bands.

(3) No source contamination within 6". The angular resolution is 6.1" and 6.4" at W1 and W2 (Wright et al. 2010). We check the SDSS image for each object to exclude source contamination.

24 CL AGNs satisfied the criterion (1) are listed in Table 1, among which, 11 objects meet the requirement (2). Finally, 10 follow all these criteria, which are named SDSS J002311.06+003517.5, SDSS J081319.34+460849.5, SDSS J090902.35+133019.4, SDSS J101152.98+544206.4, SDSS J102152.34+464515.6, SDSS J132457.29+480241.2, SDSS J155440.25+362952.0 (iPTF 16bco), SDSS J225240.37+010958.7 (here after: J002311, J081319, J090902, J101152, J102152, J132457, J155440 and J225240, respectively), Mrk 1018 and NGC 2617.

3. MID-INFRARED AND OPTICAL LIGHT CURVES

The 10 sources with significant MIR variability can be categorized into two equal subsamples depending on whether the BELs appeared or disappeared, that is changed from Type 2 to Type 1 or vise versa. Below, we will introduce the MIR and optical light curves of the two classes, respectively.

3.1. *From Type1 to Type 2*

J101152, J102152, J132457 and Mrk 1018 are reported to experience transitions from Type 1 to Type >1.8 (Runnoe et al. 2016; Macleod 2016; McElroy et al. 2016). Their CRTS and WISE light curves are presented in (a)-(d) of Fig 1. Along with the transition, all the MIR light curves show apparent dimming (> 0.4 mag) in both W1 and W2. However, only J101152 and Mrk 1018 exhibit a similar dimming trend in V-band light curves. We have tried to fit their SDSS images with PSF+Sersić model using 2-D decomposition software GALFIT (Peng et al. 2002), assuming that the PSF and Sersić represent the AGN and host galaxy emission, respectively. Our results suggest that the PSF component accounts for 26% and 42% for J102152 and J132457 in SDSS r-band, that is taken before the type transition. Due to seeing-limit, the fitted PSF component can be considered as an upper limit of the AGN, which means that the real AGN fraction is even lower and thus their optical variability is largely diluted. We have also noted that their g-band variability is much more significant ($\Delta g > 1$ mag, Macleod et al. 2016) because it's less affected by the host galaxy. J101152 is totally AGN dominated and Mrk 1018 is a nearby ($z = 0.035$) Seyfert galaxy with a well resolved nucleus, making their V-band variation are pretty detectable. We use yellow dashed and dotted lines to mark the significant/upper limit variation time scale of MIR bands of each source, see Fig 1)

Here we give some notes for each object.

(1) J101152: W1 faded by 1.10 mag within ∼4.00 yr, while W2 by 1.76 mag.

(2) J102152: In ∼4.01 yr, W1 and W2 dimmed ∼0.59 and ∼0.62 mag respectively.

(3) J132457: It showed disappearance of BELs (Macleod et al. 2016), but recently likely appears BELs (Ruan et al. 2016). Two MIR bands show similar rebrightened behavior. Both MIR bands dimmed continuously with W1 and W2 ∼0.47 and ∼0.45 mag respectively in ∼4.53 yr and then brightened after the turning point MJD≃57000.

(4) Mrk 1018: It changed from Type 1.9 to Type 1 in 1984 (Cohen et al. 1986), but recently returned to Type 1.9 (McElroy et al. 2016). In ∼4.49 yr, W1 dimmed by 0.76 mag while W2 by 1.05 mag.

3.2. *From Type 2 to Type 1*

In (e)-(h) of Fig 1, we plot J225240, J002311, J155440 and NGC 2617, which show evidence of emerging BELs (Maclead et al. 2016; Gezari et al. 2017; Shappee et al. 2014). Along with the transition, J155440 and NGC 2617 show rising trend in their MIR bands. As for J225240 and J002311, the BOSS spectrum was taken during the WISE epoch, which means their transitions happened before the WISE survey (see (e) and (f)). So the WISE and NEOWISE missed the main uptrend transition period but covered the latter period. This situation is more obvious in J081319 and J090902 which are presented in Fig 2. We note the six objects following.

(1) J225240: V-band luminosity kept increasing (ΔV>1 mag) during the transition, but decreased afterwards, indicating it might change back to a dim state. W1 and W2 exhibit very similar variations. Since there's a gap between WISE and NEOWISE, we can only derive an upper limit of decreasing time scale as 3.52 yr, with W1 and W2 dimming ~0.65 and ~0.52 mag respectively.

(2) J002311: Optical/MIR variation behavior is very similar to J2252's. The MIR bands dropped significantly in 1.51 yr (from gray dashed line to yellow dotted line), with W1 and W2 dimming ~0.41 and ~0.27 mag respectively). Due to the gap in the MIR bands, we estimate the upper limit of decreasing time scale as 4.51 yr (from yellow dashed line to yellow dotted line).

(3) J155440: It was discovered as a transient on 2016 Jun 1 by iPTF (named as 'iPTF 16bco', Gezari et al. 2017). From MJD=55409 to 57055, during ~4.51 yr W1 and W2 brightened 0.69 and 0.94 mag respectively.

(4) NGC 2617: It was a Seyfert 1.8 galaxy in 2003 but showed appearance of BELs in 2013 (Shappee et al. 2014). From MJD=55506 to 56776, during ~3.48 yr the W1 and W2 brightened 0.5 and 0.78 mag respectively.

(5) J081319 and J090902: J081319 was a Seyfet 1.8 galaxy in 2000, so was J090902 in 2006. Both of them were classified as Type 1 in 2010 (Runco et al. 2016). Their MIR bands present a remarkable drop, in contrary to their previous transition, indicating a new change. We confirmed they have changed back to Type 1.9 using the Double Spectrograph (DBSP) of the Hale 200-inch telescope at Palomar Observatory. The spectrum of J081319 was obtained on 2017 Jan 8, while J090902's on Jan 18 (see Fig 3).

In summary, MIR bands of all the objects show very similar variation to the optical data, which is in accordance with the type transition. In Fig 3, we plot W1-W2 of each sources. The sources with transition from Type 1 to 2 likely change from AGN-like MIR-color (W1-W2>0.8) to galaxy-like MIR-color (W1-W2<0.5), vise versa (Stern et al. 2012, Yan, Lin et al. 2013). We list the upper limit of MIR variation time as ΔT in column 9, the change of MIR bands $\Delta W1$ and $\Delta W2$ in column 11 and 12 of Table 2.

3.3. *Remaining objects*

Besides the 10 sources with significant MIR variability described above, we also examine the remaining targets with very weak/non-detectable MIR variations. For example, J233317.38-002303.4 and J214613.31+000930.8 which have appearance of BELs, show significant uptrend in g-band light curves but turn into plateau with little variation after MJD~54500 (Macleod et al. 2016), implying they might finish the transition. For Mrk 590, it has changed to Type 1.8~1.9 by 2006 (Denny et al. 2014). Since their MIR light curves began at MJD~55179, WISE likely missed their most significant transition epoch. For J233602.98+001728.7 and J022652.24-003916.5 their infrared radiation are too faint (W1~15.4, W2~14.8) to detect significant variation. The reasons above are applicable to most of the other objects not included in our sample, except J154507.53+170951.1, which is contaminated by other source within 6".

4. DISCUSSION

4.1. *Physical scenarios*

The main motivation of this paper is to explore the physical mechanism of CL AGNs using MIR variability. Mid-IR emission at 3.4 and 4.6μm are mainly originated from hot dust emission heated by AGNs (Netzer, 2013), hence the MIR emission should respond to the variation of accretion rate with a time delay. On the other hand, the MIR bands are little affected by dust extinction, any detectable variability means a much larger amplitude of variability in the optical if CL is caused by the changing of obscuration. Even for J002311, whose MIR variation is the weakest (ΔW2=0.27) among the 10 objects in our sample, $\Delta V \sim 6$ is required assuming the extinction model of (Fitzpatrick et al. 1999). Such a dramatic optical variability is extremely rare for AGNs and doesn't agree with the optical light curves here.

Nevertheless, we further investigate the dynamical time scale of the obscuration. The size of the obscurer should be at least comparable to the torus to block the hot dust. With the inner radius of the torus simply estimated from the dust sublimation radius (Netzer, 2013, $R_{sub} = 0.5L_{46}^{0.5}(1800K/T_{sub})$ pc), the crossing time for the obscuring material can be derived as $t_{cross} = 0.073[r_{orb}/(lt-day)]^{3/2}M_8^{-0.5}arcsin(r/r_{orb})$ yr (LaMassa et al. 2015), where r_{orb} is the circular orbital radius of the obscurer, M_8 is the mass of black hole in units of $10^8 M_\odot$, and r is the true size of the obscured region (i.e. continuum emitting region or BLR size). We adopted r as the BLR size, which are estimated from calibrated $R-L$ relation (Bentz et al. 2013) and the calculated R_{sub} and t_{cross} are listed in Table 2 (column 6 and 8). It can be seen clearly that t_{cross} is much longer than the observed MIR variation time ΔT for all the 10 objects.

Based on the analysis above, the CL behavior of our sample can not be a result of the changes in obscuration. Once the obscuration case is ruled out, the MIR variability can be naturally attributed the hot-dust echo of the dramatic changing of the accretion rate. The time delay of the MIR and optical variability can offer us a unique opportunity to measure the radius of the torus. Previous studies basing on K-band reverberation mapping suggested $R_{in} = R_{\tau_K} = 0.47(L_{\rm bol}/10^{46}{\rm erg\ s^{-1}})^{0.5}$ (Suganuma et al. 2006). Assuming $R_\lambda = (\lambda/\lambda_K)^2 R_{\tau_K}$, we got $R_{\rm W1} = 0.36$ pc (0.11 pc) and $R_{\rm W2} = 0.67$ pc (0.21 pc) for $\log L_{bol} = 45$ erg s^{-1}(44 erg s^{-1}), corresponding to time lag of 2.18 yr (0.68 yr) in the rest-frame, or 1~3 yr in the observed-frame. We have tried to shift the MIR light curves backward a few of years, their variation pattern really match the optical ones well, giving fantastic evidence for the dust echo response to the accretion. In summary, we conclude that all of the 10 CL AGNs with significant MIR variability have undergone an drastic drop/rise in accretion rate.

4.2. *More information from the infrared variation*

The MIR light curves can not only help us diagnose the physical scenarios of CL AGNs, but also allow us to get more transition information, and even predict new CL behaviors. Because MIR bands are AGN-heated hot dust dominated, they're more efficient to detect when the AGN is optically weak comparable to its host galaxy (e.g. J102152 and J132457 in §3.1). For J155440, it was proposed that the turn on change state has occurred less than 500 days before 2016 Jun 1 (Gezeri et al. 2017. However, according to the V-band and the MIR-band light curves, the 'turn on' event much likely began around Jun 2013 $\sim$ Feb 2014 (marked by purple dotted lines,see (g) of Fig 1). The two objects J081319 and J090902 presented very similar sign of new transition due to the MIR decline and we confirmed they had changed back to Type 1.9. For J225240 and J002311, which changed from Type 2 like to Type 1, show a dramatical decline in MIR and optical light curves, suggesting they might also have changed back to type 2. We're planing to perform follow-up spectral observations to confirm of our conjecture.

5. CONCLUSION

We investigate the 10 reported CL AGNs confirmed in optical spectrum in literature. Combining with WISE and NEOWISE multi-epoch photometric data (W1, W2), all the 10 sources have obvious MIR variation (> 0.4 mag) at level $> 10\sigma$. The obscurer passing across the line of sight could not cause such large variation, due to the extinction and dynamical obscuration time-scale of which are failed to support it. 4 sources with disappearance of BELs, namely J101152, J102152, J132457, Mrk 1018, show similar significant decline ($> 10\sigma$) in MIR light curves which echo to the optical variation. We suggest that their CL is owing to a drop in accretion rate. Among the 4 sources showing emerging of BELs, 2 objects J155440 and NGC 2617 feature remarkable increase feature in MIR luminosity, in accordance with their transition and also the V-band increasing tendency. We suggest their CL is due to rising up of the accretion rate. And other two named J225240 and J002311, abnormally display significant decrease in MIR bands, indicating they might undergo a second transition and change back to the previous Type 2, which should be confirmed by follow-up observation. Especially, J081319 and J090902 which are reported changed from type 1.8 to type 1, have significant ($> 10\sigma$) decrease MIR signals. We have confirmed they had changed back to type 2. Further and repeat spectroscopic monitor of sources with large MID-infrared variability sources could be worthy.

ACKNOWLEDGMENTS

We acknowledge the anonymous referee for valuable comments helping to improve the paper. And we acknowledge Andrew Drake for providing the unreleased CRTS data (Drake et al. 2009) of J155440. Also we acknowledge Jordan N. Runco for helpful information of J081319 (Runco et al. 2016). We will thank Luming Sun for discussion and thank Zhihao Zhong for his perfect spectrum reduction skill. This project is supported by National Basic Research Program of China (grant No. 2015CB857005), the NSFC through NSFC-11233002, NSFC-11421303, and U1431229, jointly supported by Chinese Academy of Science and NSF. This research has made use of the NASA/ IPAC Infrared Science Archive, which is operated by the Jet Propulsion Laboratory, California Institute of Technology, under contract with the National Aeronautics and Space Administration. The CSS survey is funded by the National Aeronautics and Space Administration under Grant No. NNG05GF22G issued through the Science Mission Directorate Near-Earth Objects Observations Program. The CRTS survey is supported by the U.S.National Science Foundation under grants AST-0909182. This research made use of Astropy, a community-developed core Python package for Astronomy (Astropy Collaboration, 2013).

REFERENCES

Abazajian, K. N., Adelman-McCarthy, J. K., Agüeros, M. A., et al. 2009, ApJS, 182, 543-558
Antonucci, R. 1993, ARA&A, 31, 473
Antonucci, R. R. J., & Miller, J. S. 1985, ApJ, 297, 621
Astropy Collaboration, Robitaille, T. P., Tollerud, E. J., et al. 2013, A&A, 558, A33
Bentz, M. C., Denney, K. D., Grier, C. J., et al. 2013, ApJ, 767, 149
Bianchi, S., Panessa, F., Barcons, X., et al. 2012, MNRAS, 426, 3225
Cohen, R. D., Puetter, R. C., Rudy, R. J., Ake, T. B., & Foltz, C. B. 1986, ApJ, 311, 135
Denney, K. D., De Rosa, G., Croxall, K., et al. 2014, ApJ, 796, 134
Drake, A. J., Djorgovski, S. G., Mahabal, A., et al. 2009, ApJ, 696, 870
Fitzpatrick, E. L., & Massa, D. 1999, ApJ, 525, 1011
Gezari, S., Hung, T., Cenko, S. B., et al. 2017, ApJ, 835, 144
Greene, J. E., & Ho, L. C. 2005, ApJ, 630, 122
Goodrich, R. W. 1989, ApJ, 340, 190
Jiang, N., Dou, L., Wang, T., et al. 2016, ApJ, 828, L14
Jiang, N., Zhou, H.-Y., Ho, L. C., et al. 2012, ApJ, 759, L31
Jun, H. D., Stern, D., Graham, M. J., et al. 2015, ApJ, 814, L12
Khachikian, E. Y., & Weedman, D. W. 1971, ApJ, 164, L109
LaMassa, S. M., Cales, S., Moran, E. C., et al. 2015, ApJ, 800, 144
MacLeod, C. L., Ross, N. P., Lawrence, A., et al. 2016, MNRAS, 457, 389
Mainzer, A., Bauer, J., Cutri, R. M., et al. 2014, ApJ, 792, 30
McElroy, R. E., Husemann, B., Croom, S. M., et al. 2016, A&A, 593, L8
Netzer, H. 2013, The Physics and Evolution of Active Galactic Nuclei, by Hagai Netzer, Cambridge, UK: Cambridge University Press, 2013,
Oknyansky, V. L., Gaskell, C. M., Huseynov, N. A., et al. 2017, MNRAS, 467, 1496
Osterbrock, D. E. 1977, ApJ, 215, 733
Osterbrock, D. E. 1981, ApJ, 249, 462
Peng, C. Y., Ho, L. C., Impey, C. D., & Rix, H.-W. 2002, AJ, 124, 266
Penston, M. V., & Perez, E. 1984, MNRAS, 211, 33P
Pons, E., & Watson, M. G. 2014, A&A, 568, A108
Ruan, J. J., Anderson, S. F., Cales, S. L., et al. 2016, ApJ, 826, 188
Runco, J. N., Cosens, M., Bennert, V. N., et al. 2016, ApJ, 821, 33
Runnoe, J. C., Cales, S., Ruan, J. J., et al. 2016, MNRAS, 455, 1691
Shappee, B. J., Prieto, J. L., Grupe, D., et al. 2014, ApJ, 788, 48
Shen, Y., Richards, G. T., Strauss, M. A., et al. 2011, ApJS, 194, 45
Shi, Y., Rieke, G. H., Smith, P., et al. 2010, ApJ, 714, 115
Stern, D., Assef, R. J., Benford, D. J., et al. 2012, ApJ, 753, 30
Suganuma, M., Yoshii, Y., Kobayashi, Y., et al. 2006, ApJ, 639, 46
Wright, E. L., Eisenhardt, P. R. M., Mainzer, A. K., et al. 2010, AJ, 140, 1868-1881
Yan, L., Donoso, E., Tsai, C.-W., et al. 2013, AJ, 145, 55

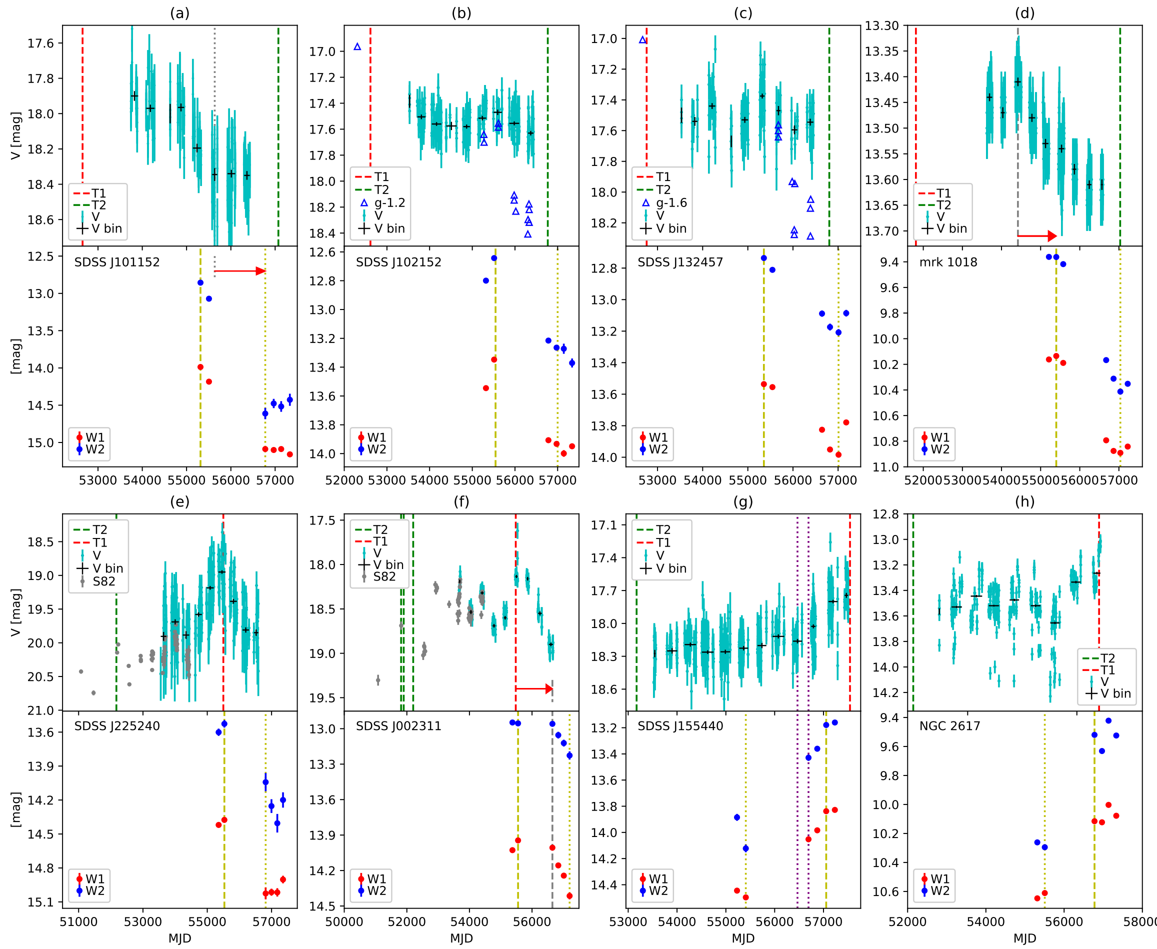

Figure 1. Changing-look AGNs with disappearing BELs:(a) J101152, (b) J102152, (c) J132457, (d) Mrk 1018; AGNs with emerging BELs: (e) J225240, (f) J002311, (g) J155440, (h) NGC 2617. In each top panel,the cyan dots with error bars are V-band data from CRTS. The black cross represent the median value of each season epoch while the y-error bars are calculated by error propagation method. The red dashed line marks the epoch of the spectrum used to confirm Type 1 (T1) while the green dashed line marks the epoch of spectrum used confirm Type 2 (T2). For J102152 and J132457, the blue empty triangles are g-band data from Macleod et al (2016). The gray dots represent the g-band data of Strip 82 (Abazajian et al. 2009) with constant offset m_0. In each bottom panel, the red and blue dots represent median value of W1 and W2 bands respectively, while the corresponding error bars are also the propagation error. The yellow dashed/dotted lines not only mark the bright/dim state of each source respectively, but also mark the start/end of the significant MIR variation time scale. The red arrow marks the upper limit lag shift between optical and MIR light curves. For J155440, the purple dotted lines mark the time range of the 'turn on' event occurred. J225240 is very dim in V-band, so we constrain the CRTS measurement error ≤0.4 when performing data processing.

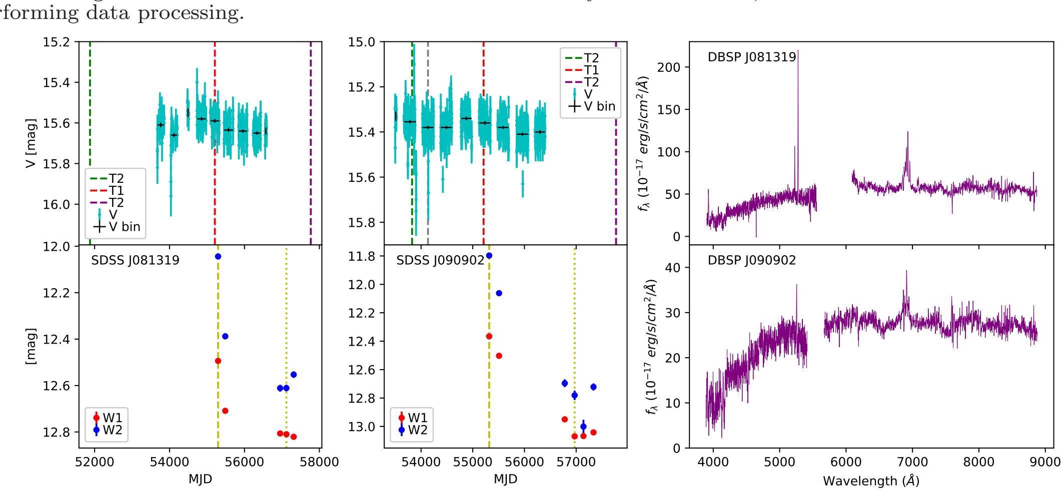

Figure 2. Light curves and spectra of J081319 and J090902. The purple dashed line marks the epoch of DBSP spectrum which confirms the second transition. Other symbols are the same as those in Fig 1. The right panel presents the spectra obtained with DBSP (We used a 600/4000 grating for the blue side and a 316/7500 grating for the red side, and a D55 dichroic was selected. The slit was 1.5" and exposure time was 10 min. The spectroscopic data were reduced following the IRAF standard routine.)

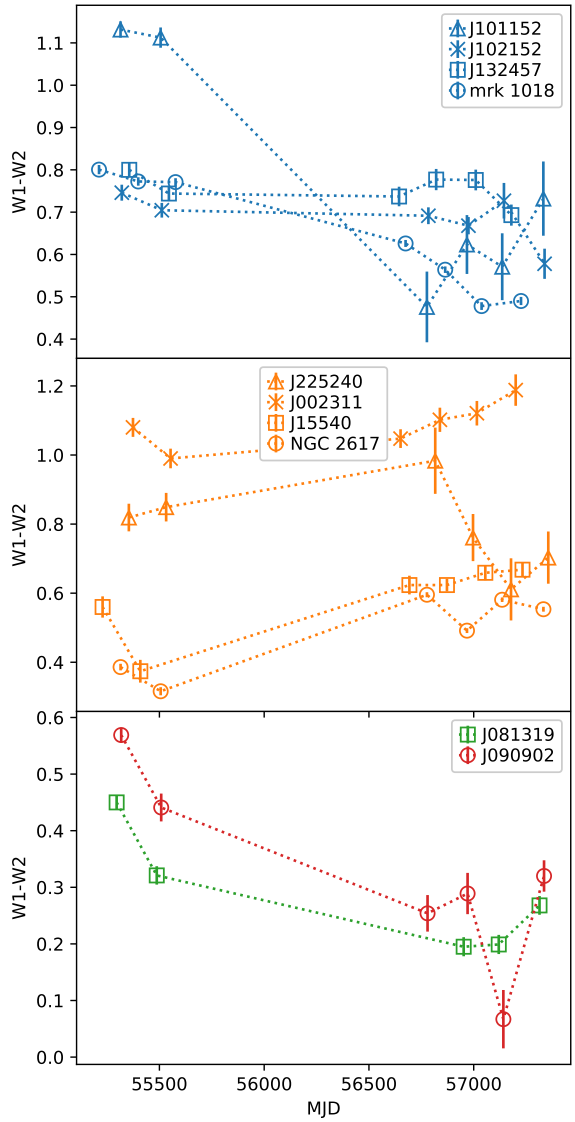

Figure 3. Color change of Changing-look AGNs. Upper panel: changing from Type 1 to Type 2 like; middle panel: changing from Type 2 like to Type 1; bottom panel: J0813 and J0909.

Table 1

(1) Name	(2) t_{spec} (MJD)	(3) $\Delta t_{wise-spec}$ (yr)	(4) Max ΔW1 (mag)	(5) Max ΔW2 (mag)	(6) σ_{W1}	(7) σ_{W2}	(8) transition	(9) note
J002311.06+003517.5	51816, 55480	-0.29	0.47±0.03	0.28±0.04	13.62	6.89	A BELs	Macleod et al. (2016)
J015957.64+003310.4	51871, 55201	0.03	0.21±0.06	0.26±0.12	3.67	2.28	D BELs	LaMassa et al. (2015)
J012648.08-083948.0	52163, 54465	2.53	0.06±0.04	0.16±0.08	1.72	1.87	D BELs	Ruan et al. (2016)
J022556.07+003026.7	52944, 55445	-0.11	0.23±0.04	0.39±0.12	5.31	3.30	D & A BELs	Macleod et al. (2016)
J022652.24 -003916.5	52641, 56267	-2.88	0.23±0.06	0.48±0.14	3.53	3.53	D BELs	Macleod et al. (2016)
J035301.02 -062326.3	51908, 54853	1.05	0.18±0.02	0.24±0.03	10.36	9.14	1.8 → 1	Runco et al. (2016)
J081319.34+460849.5	51877, 55210	0.24	0.33±0.01	0.57±0.02	27.47	31.42	1.8 → 1	Runco et al. (2016)
J084748.28+182439.9	53711, 54852	1.26	0.29±0.01	0.34±0.02	22.19	14.93	1 → 1.9 → 2	Runco et al. (2016)
J090902.35+133019.4	53826, 55210	0.29	0.70±0.02	1.20±0.05	41.98	24.57	1.8 → 1	Runco et al. (2016)
J093812.27+074340.0	52733, 55210	0.32	0.04±0.01	0.07±0.01	4.26	4.76	1 → 1.8	Runco et al. (2016)
J094838.43+403043.5	52709, 55211	0.29	0.19±0.01	0.16±0.01	20.94	15.41	1 → 1.8	Runco et al. (2016)
J100220.17+450927.3	52376, 56683	-3.74	0.30±0.03	0.26±0.06	9.36	4.58	D BELs	Macleod et al. (2016)
J101152.98+544206.4	52652,57073	-4.82	1.17±0.04	1.76±0.08	33.19	22.69	D BELs	Runnoe et al. 2016
J102152.34+464515.6	52614, 56769	-3.97	0.65±0.03	0.73±0.03	25.68	21.27	D BELs	Macleod et al. (2016)
J132457.29+480241.2	52759, 56805	-3.97	0.45±0.02	0.47±0.02	27.55	17.65	D BELs	Macleod et al. (2016)
J154507.53+170951.1	53889, 54936	0.82	0.53±0.01	0.66±0.01	49.72	47.89	1.8 → 1	Runco et al. (2016)
J155440.25+362952.0	53172,57543	-6.34	0.67±0.02	0.96±0.03	35.93	27.76	2→1	Gezari et al. (2017)
J214613.31+000930.8	52968, 55478	-0.39	0.14±0.04	0.13±0.06	3.48	2.20	A BELs	Macleod et al. (2016)
J225240.37+010958.7	52174, 55500	-0.40	0.65±0.06	0.88±0.09	11.26	9.93	A BELs	Macleod et al. (2016)
J233317.38 -002303.4	52199, 55447	-0.23	0.28±0.04	0.14±0.05	7.45	2.81	A BELs	Macleod et al. (2016)
J233602.98+001728.7	52096, 55449	-0.23	0.40±0.08	0.71±0.25	5.20	2.78	D BELs	Ruan et al. 2016
Mrk 590	52649, 56664	-3.97	0.13±0.01	0.34±0.01	18.61	43.95	1.5 → 1 → 2	Denney et al. (2014)
Mrk 1018	51812, 57033	-4.99	0.76±0.01	1.05±0.01	79.92	105.78	1.9 → 1 → 1.9	McElroy et al. (2016)
NGC 2617	53003, 56407	-2.99	0.64±0.01	0.87±0.01	74.38	93.95	1.8 → 1	Shappee et al. (2014)

Note. — The information of 24 CL AGNs. t_{spec} lists the MJD of two spectrum be used to confirm the type transition; $\Delta t_{wise-spec}$ lists the interval between first WISE data point and the spectrum epoch (second MJD in t_{spec}) which confirmed transition ($\Delta t_{wise-spec} < 0$ means that the transition is more likely to to be covered by WISE/NEOWISE); column 4 and 5 list the maximum variation of W1 and W2 bands, while column 6 and 7 are the corresponding variation significance of W1 and W2; column 8 lists the transition of each source, 'A' BELs means appear BELs, while 'D' BELs means disappear BELs; last column lists the corresponding paper

Table 2

(1) Name	(2) z	(3) $\log M_{BH}/M_{\odot}$	(4) $\log L_{bol}$ (erg s^{-1})	(5) $\log L_{5100}$ (erg s^{-1})	(6) R_{sub} (pc)	(7) R_{BLR} (lt-day)	(8) t_{cross} (yr)	(9) ΔT (yr)	(10) R_{torus} (pc)	(11) $\Delta W1$ (mag)	(12) $\Delta W2$ (mag)
J002311.06+003517.5	0.422	9.23	45.480	44.513	0.275	63.16	28.95	4.51	0.69	0.41	0.27
J101152.98+544206.4	0.246	7.78	45.117	44.150	0.181	40.45	69.96	4.00	-	1.10	1.76
J102152.34+464515.6	0.204	8.33	45.121	44.154	0.182	40.65	36.16	4.01	0.81	0.59	0.62
J132457.29+480241.2	0.272	8.51	45.303	44.336	0.224	50.83	43.11	4.53	-	0.45	0.47
J155440.25+362952.0	0.237	8*	45.146*	44.23*	0.187	44.63	60.61	4.51	-	0.66	0.94
J225240.37+010958.7	0.534	8.88	45.318	44.352	0.228	51.83	34.93	3.52	-	0.65	0.52
Mrk 1018	0.035	7.4∼7.9*	44.491*	-	0.088	24*	21.0∼37.4	4.49	0.82	0.76	1.05
NGC 2617	0.00142	7.6*	44.03*	43.12*	0.05	11.42	10.4	3.48	-	0.50	0.78
J081319.34+460849.5	0.054	6.98∼7.28⋆	43.56∼44.01⋆	42.65∼43.10⋆	0.03∼0.05	6.44∼11.14	9.57∼15.34	5.00	-	0.32	0.57
J090902.35+133019.4	0.050	7.03∼7.32⋆	43.42∼43.87⋆	42.51∼42.96⋆	0.03∼0.04	5.43∼9.39	7.06∼11.31	4.53	-	0.70	0.98

Note. — The table lists redshift, black hole mass, bolometric luminosity, monochromatic luminosities at 5100Å and sublimation radius R_{sub} of each source in 2∼6 columns. The estimated characteristic radius of BLR and crossing time scale t_{cross}(in observation frame) for obscuration, along with the observed MIR variation time scale ΔT are listed in 7∼9 columns. The column 10 lists the estimated upper limit of the radius of torus. Column 11 and 12 list the change of MIR bands. The luminosities, redshift and M_{BH} are taken from Shen et al. 2011, except the data with a asterisk annotation are from the corresponding paper of which the source is reported, and the data with a star annotation are estimated from Hα (Greene et al. 2005) by fitting the SDSS spectrum.